Nanochemistry: Synthesis and Characterization of Multifunctional Nanoclinics for Biological Applications

Laurent Levy, Yudhisthira Sahoo, Kyoung-Soo Kim, Earl J. Bergey, and Paras N. Prasad*

Institute for Lasers, Photonics and Biophotonics, Natural Sciences Complex, Department of Chemistry, State University of Buffalo at New York, Buffalo, New York 14260-3000

Received March 28, 2002. Revised Manuscript Received July 2, 2002

This paper presents the use of nanoscale chemistry to synthesize a multilevel, hierarchically built nanoparticle, which we define as a nanoclinic, for targeted diagnostics and therapy. This nanoclinic, produced by multistep chemistry in a nanosize micelle, consists of a thin silica shell encapsulating magnetic (Fe_2O_3) nanoparticles and fluorescent dyes for enhanced contrast magnetic resonance and optical imaging and magnetic-induced cancer therapy. Furthermore, the surface of these prototype nanoclinics is functionalized with a biotargeting group, luteinizing hormone-releasing hormone (LH−RH). In the work reported here, the LH−RH targets receptor-specific cancer cells for utilization in imaging and investigation of biological effects. The structure and function of these nanoclinics have been characterized using electron and X-ray diffractions, transmission electron microscopy, atomic force and scanning electron microscopy and two-photon laser scanning microscopy. Targeting of the receptor-specific cells has been demonstrated, along with the demonstration of a new mechanism of selective destruction of cancer cells, in a dc magnetic field, using these magnetic nanoclinics.

Introduction

Nanochemistry holds tremendous promise for new approaches in medical diagnostics and disease therapy. Examples of this technology include nanocrystal fluorophores for imaging, nanoscale biodevices as sensors, and nanobubbles for drugs delivery.[1−4] In cellular research, the PEBBLE nanotechnology of Kopelman and co-workers enables for the optical measurement of changes in intracellular calcium levels and pH and has provided a major advancement in the field of nanoprobes and nanomedicine.[5,6] In this paper, we present another new dimension to targeted diagnosis and therapy using nanoclinics that are produced by multistep nanochemistry using a micellar system. These nanoparticles are subsequently surface-functionalized to target specific cells or biological sites. These nanoclincis are ≤50-nm silica shells that can encapsulate various optical, magnetic, or electric probes as well as platforms containing externally activatable drugs or therapeutic agents (see Figure 2A for a schematic representation). The size of these nanoclinics is small enough to enter the cell in order for them to function from within the cell.

In the work reported here, the silica shell of the nanoclinic is formed by sol−gel chemistry within a micelle cavity of an appropriately chosen and precisely controlled dimension. This shell encloses magnetic nanoparticles of Fe_2O_3 and a two-photon dye. Then the surface of these silica shells is functionalized to attach bioreactive groups to target them to specific biological sites (a specific cancer cell in the present case). In the study reported here, the targeting group is a hormone analogue of LH−RH. The structure and properties of these nanoclinics are characterized by using electron diffraction, X-ray diffraction, transmission electron microscopy, and atomic force microscopy. Targeting of LH−RH receptor-specific cancer cells and specific effect of these prototypic nanoclinics are demonstrated.

The present work also reports a new discovery, that is, selective lysing of cancer cells in a dc magnetic field using magnetic nanoclinics. Magnetic probes or particles have been investigated for a potential alternative treatment for cancer. Studies have demonstrated that the hyperthermic effect generated by magnetic particles coupled to a high-frequency ac magnetic field (requiring tremendous power) could be used as an alternate or adjuvant to current therapeutic approaches for cancer treatment.[7−10] This hyperthermic effect (heat produced by the relaxation of magnetic energy of the magnetic material) was shown to effectively destroy tumor tissue surrounding the probes or particles. This approach resulted in reduction of tumor size by this effect when

* To whom correspondence should be addressed.

(1) Kreuter, J. *J. Anat.* **1996**, *189*, 503.
(2) Kreuter, J. *Pharm. Biotechnol.* **1995**, *6*, 463.
(3) Rosen, B. R.; Brady, T. J. *J. Comput. Assist. Tomog.* **1993**, *17*, S36.
(4) Tibbe, A. G.; de Grooth, B. G.; Greve, J.; Liberti, P. A.; Dolan, G. J.; Terstappen, L. W. *Nat. Biotechnol.* **1999**, *17*, 1210.
(5) Clark, H. A.; Kopelman, R.; Tjalkens, R.; Philbert, M. A. *Anal. Chem.* **1999**, *71*, 4837.
(6) Clark, H. A.; Hoyer, M.; Philbert, M. A.; Kopelman, R. *Anal. Chem.* **1999**, *71*, 4831.
(7) Yanase, M.; Shinkai, M.; Honda, H.; Wakabayashi, T.; Yoshida, J.; Kobayashi, T. *Jpn. J. Cancer Res.* **1998**, *89*, 775.
(8) Hilger, I.; Bahring, R.; Daum, A.; Hergt, R.; Kaiser, W. A. *Invest. Radiol.* **1997**, *32*, 705.
(9) Schutt, W.; Gruttner, C.; Hafeli, U.; Zborowski, M.; Teller, J.; Putzar, H.; Schumichen, C. *Hybridoma* **1997**, *16*, 109.
(10) Tohnai, I.; Goto, Y.; Hayashi, Y.; Ueda, M.; Kobayashi, T.; Matsui, M. *Int. J. Hypertherm.* **1996**, *12*, 37.

10.1021/cm0203013 CCC: $22.00
Published on Web 08/09/2002

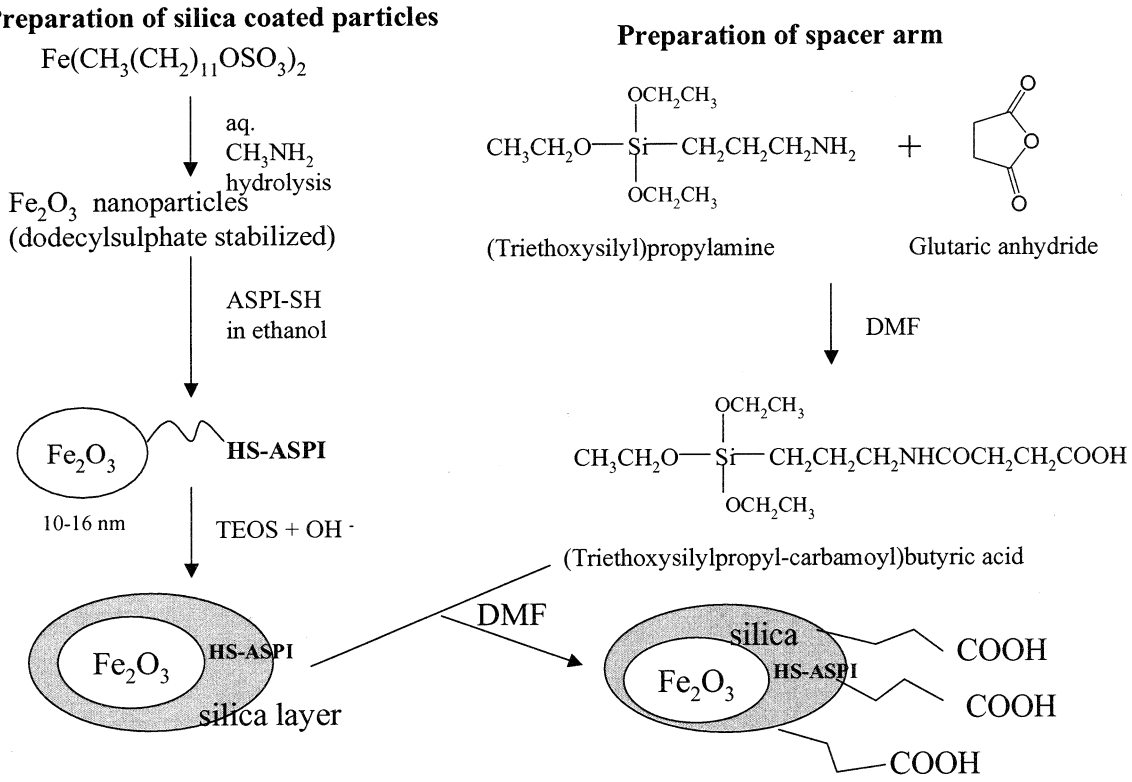

Figure 1. Schematic diagram of synthetic protocol.

the particles were directly injected into the tissue and were exposed to an alternating magnetic field.[9] However, no targeted therapy using a dc magnetic field has been reported to our knowledge. We, therefore, believe our report to be the first to demonstrate the use of a dc magnetic field at a strength typically achievable by magnetic resonance imaging (MRI) systems for selectively destroying cancer cells.

Experimental Procedure

Materials. 3-(Triethoxylsilyl)propylamine, tetraethyl orthosilicate (TEOS), benzotriazolyl-*N*-oxytrisdimethylaminophosphonium hexafluorophosphate (BOP), and *N*,*N*-diisopropylethylamine (DIPEA) were obtained from Aldrich Chemical Co., Milwalkee, WI. LH−RH (D-Lys[6]) was obtained from Sigma Chemical Co., St Louis, MO. ASPI−SH fluorophore was prepared in our laboratory as described by Lal et al.[11] KB and CV-1 cells lines were obtained from the American Type Cell Collection (ATCC), Rockville, MD. Cells were grown and maintained as per recommendation by the ATCC.

Nanoclinic Synthesis. A multistep process was used for the fabrication of nanoclinics. First, the synthesis of iron dodecyl sulafate {$Fe(DS)_2$} was accomplished through the addition of $FeCl_2 \cdot 4H_2O$ (6.36 g) to 400 mL of water at 50 °C followed by sodium dodecyl sulfate (2.3 g) and the solution was stirred for 2−3 h. This solution was then cooled to 4 °C and stored for 24 h. The precipitate was collected by filtration and washed with cold water. The surfactant was dried for 2−3 days under vacuum. The synthesis of the Fe_2O_3 magnetic core was performed using a colloidal reaction described by Feltin and Pileni.[12] $Fe(DS)_2$ (180 mg) and methylamine (2.4 mL) were added to 40 mL of distilled water and stirred vigorously for 3 h at 80 °C. The solution was cooled to room temperature and a three-quarter portion was retained for the studies involving TEM, XRD, and magnetization of the particles thus formed.

(11) Lal, M.; Levy, L.; Kim, K. S.; He, G. S.; Wang, S.; Min, Y. H.; Pakatchi, S.; Prasad, P. N. *Chem. Mater.* **2000**, *12*, 2632.
(12) Feltin, N.; Pileni, M. P. *Langmuir* **1997**, *13*, 3927.

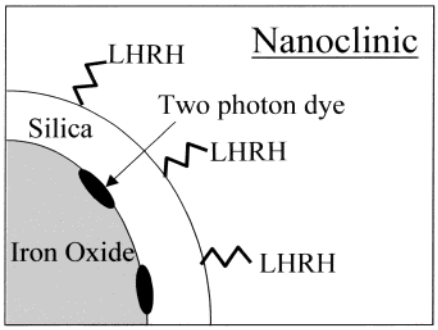

Figure 2. Schematic representation of a LH−RH nanoclinic.

The other portion was heated to 45 °C and the two-photon dye, ASPI−SH (0.2 M in alcohol, 1 mL), was added to the ferrofluid solution and the solution incubated at room temperature for 4 h under vigorous stirring. To produce the silica layer and prevent aggregation due to magnetic interaction, sodium silicate was added to the solution (5 μL/10 mL of solution). The suspension was stirred for 24 h at room temperature with ultrasonic bath sonication for 5 min every 4 h. The particles were washed in 1:2 ethanol:water at pH 8.5−9 and particles collected by centrifugation (10000*g*). Washed particles were redispersed in a 4:1 solution ethanol:water and 200 μL of 0.1 M NH_4OH was added. TEOS (20−200 μl) was added to the particle suspension under stirring. After 14 h, particles were washed as above in preparation for the addition of a spacer arm for attachment of LH−RH. 3-(Triethoxylsilylpropylcarbamoyl)butyric acid (spacer arm) was prepared by incubating 3-(triethoxylsilyl)propylamine (4.5 mmol) with 4.5 mmol of glutaric anhydride in 1 mL of anhydrous DMF. The resulting product was dispersed in DMF containing 40 mg of particles. After the solution was stirred for 24 h at room temperature, the particles were washed with DMF and dried. The synthetic scheme is represented in Figure 1. The COOH-coated nanoclinics (2 mg) were dispersed in 1 mL of anhydrous DMF using sonication. The coupling of the peptide hormone analogue, LHRH (D-Lys[6]), was accomplished as described by Wang et

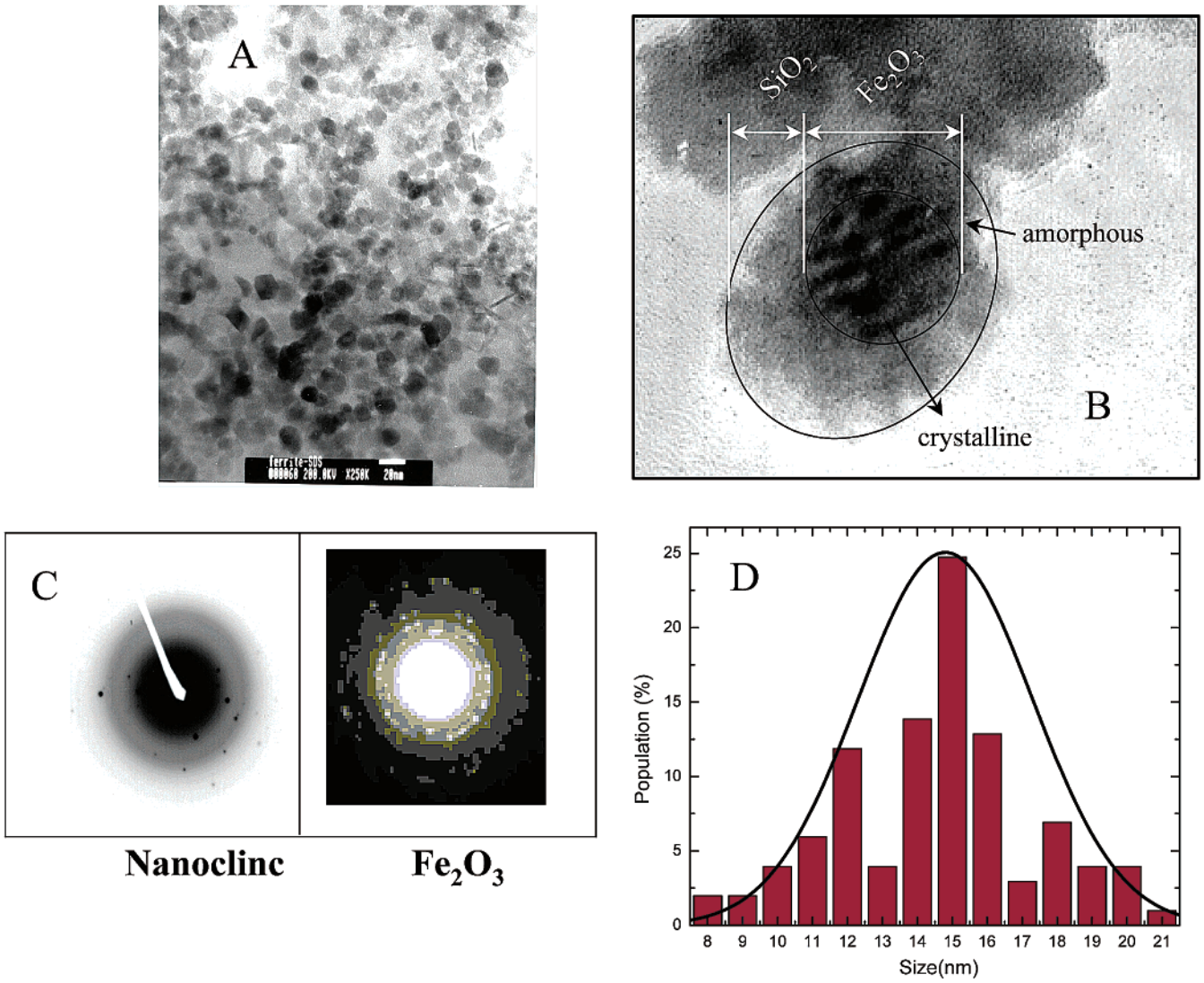

Figure 3. Transmission electron microscopy. (A) TEM of a collection of particles and their statistics. (B) High-resolution TEM image of a nanoclinic showing the core/shell structure (with corresponding structured and unstructured patterns). (C) Electron diffractions of Fe_2O_3 particles and nanoclinics (dots correspond to structured Fe_2O_3 material and diffused lines to SiO_2 shell). (D) Size distribution of nanoclinic cores.

al.[13] LH−RH (2 mg) and 24 mg of BOP were added to the suspension and sonicated for 5 h at room temperature. To neutralize any reactive groups on the nanoclinics, 100 μL of DIPEA was added dropwise to the solution and sonicated as above. The product was collected by centrifugation (10000*g*) and washed with DMF and water. For better stability, the particles were dispersed in a large volume of water containing 10% DMSO and concentrated when needed for experiments.

Transmission electron microscopy and electron diffraction were performed using a Model 200 JEOL microscope at an acceleration voltage of 200 kV in the bright field image mode. A drop of the nanoparticle solution was cast on a 300-mesh copper grid coated with amorphous graphite and allowed to dry. X-ray diffraction was taken on a Siemens X-ray diffractometer model D500 with a Cu Kα source. The 2θ angles probed were from 3° to 60° at a rate of 2°/min.

Magnetization of the bare particles in the ferrofluid phase was measured by a Quantum Design MPMS C-151 SQUID magnetometer. The magnetic field was ramped from 0 to 4000 G at 310 K and magnetization of the ferrofluid was totally saturated at this field.

(13) Wang, X.; Krebs, L. J.; Al-Nuri, M.; Pudavar, H. E.; Ghosal, S.; Liebow, C.; Nagy, A. A.; Schally, A. V.; Prasad, P. N. *Proc. Natl. Acad. Sci.* **1999**, *96*, 11081.

Characterization of Cellular Interaction of Nanoclinics. Nanoclinics were incubated with adherent KB cells (oral epithelial carcinoma; LH−RH receptor positive) or CV1 cells (green African monkey kidney cells; LH−RH receptor negative) at room temperature. Two-photon laser scanning microscopy was performed using a BioRad (Model 1024) confocal microscope coupled to a diode-pumped vandidate laser (Millenia) and pumped Ti-sapphire (Tsunami) dye laser, providing femtosecond pulses at 800 nm for two-photon excitation. Images were recorded in a growth medium at room temperature using a 60X water immersion objective. Nanoclinics (20−25 pg of dry weight/1000 cells) were added to cell monolayers and optical sections of cells were obtained after 15 min of incubation.

Magnetocytolysis. Nanoclinics (20 pg/1000 cells) were incubated on adherent KB cells for 2 h at 37 °C. Cells were trypsinized, redispersed in buffer, and exposed for 20 min to a 7 T dc magnetic field. Reduction of cell number was determined by counting cells using a hemocytometer. Cell viability was determined using trypan blue exclusion. Cell enumeration after exposure resulted in a 30−85% loss in the cell number depending on experimental conditions, when compared to control experiments (CV-1 cells lacking LH−RH receptor or use of control nanoclinics lacking LH−RH).

Atomic Force Microscopy and Scanning Electron Microscopy. Nanoparticles were incubated for 2 h at 37 °C

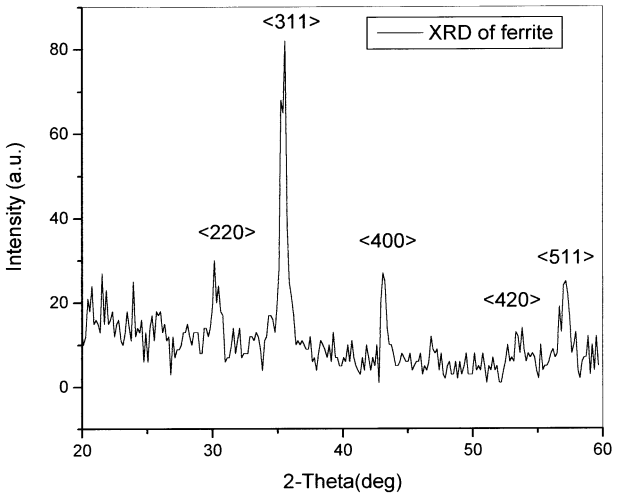

Figure 4. X-ray diffraction spectrum of an Fe_2O_3 powder sample. Lines represent theoretical X-ray patterns for the maghemite structure. The diffraction peaks are indexed for a fcc phase.

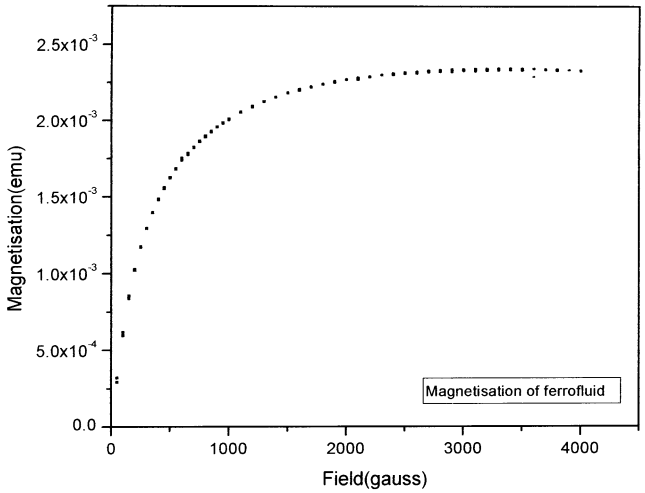

Figure 5. Magnetization vs field of a ferrofluid Fe_2O_3 sample. Magnetization saturates at 4000 G.

with adherent cells. The medium was removed and the cells were washed several times with PBS and fixed with 1% glutaraldehyde in PBS. Fixed cells were washed with water, air-dried at room temperature for 24 h, and imaged on a BioScope (Digital Instruments, CA) using tapping mode at a scan rate of 1 Hz using silicon tips (10-nm diameter). For SEM, nanoclinics were incubated for 2 h at 37 °C with adherent cells. The medium was removed and the cells were washed several times with phosphate buffered saline (PBS) and fixed with 1% glutaraldehyde in PBS. Cells were dehydrated by graded alcohol washing before imaging.

Results

Characterization and Properties of Nanoclinics. The overall schematic of the structure of the nanoclinic is represented in Figure 2. Transmission electron microscopy (TEM) of nanoclinics shows that they were found to be fairly well separated, but also in some areas aggregates of larger particles are evident (Figure 3A). In Figure 3B, we show a high-resolution TEM picture of a single particle with the Fe_2O_3 core and silica shell, the lattice fringes of the core being clearly visible. A statistical analysis of the size of the nanoclinics, employing an image-processing software developed by Scion Corp., determined that the core diameters of these nanoparticles vary from 10 to 20 nm with a median of 15 nm (Figure 3D). For the purpose of our present study, it is not essential to have uniformly sized particles and hence polydispersity is tolerated without any attempt for selective size fractionation. The electron diffraction pattern shows a crystalline structure of the nanoparticles. The core diameter was found to be 18 nm with the silica shell adding an additional thickness of 7 nm, thus making an average diameter of 32 nm for the nanoclinic. The electron diffraction of the bare Fe_2O_3 particles and that of the nanoclinic show purely crystalline and mixed (crystalline plus amorphous) patterns, respectively (Figure 3C).

X-ray Diffraction. The diffractogram (Figure 4) shows peaks corresponding to a fcc cubic maghemite structure. From the *d* values of the peaks, the estimated lattice parameter is 8.339 Å, consistent with the literature value.[14] Using Mossbauer spectral data, it has been reported by Feltin and Pileni[12] that the composition of largely Fe_3O_4 particles produced by the above method changes to Fe_2O_3 with aging. In our case, we may have a mixture of both the oxides. But because of the fact that both these oxides are magnetic, it was not considered important to determine the relative percentages of these phases in our sample. Further, the surface states of either phase would allow the growth of a silica shell. It is reasonable to believe that our sample would largely be made of Fe_2O_3 because of the open-to-atmosphere preparation and handling procedures.

Magnetization. The ferromagnetic response for the Fe_2O_3 nanoparticles was found (Figure 5) with the magnetization saturating at a field of 4000 G. A preliminary run with field reversal exhibited hysteretic magnetization behavior at room temperature for the free nanoparticles as well as for the ones bound to cells (not shown in figure). Our particles with an average diameter of 16 nm are right at the fringe of the superparamagnetic limit.[15] Ferromagnetic rather than superparamagnetic behavior could emerge from multidomain structures in the particles and/or because of interparticle interaction within the magnetic fluid volume. A switch from superparamagnetic to ferromagnetic response in the Fe_2O_3 ferrofluid has been reported when the particle sizes increased from an average size of 8.3 nm to an average size of 11.6 nm.[12] On the other hand, Hatton and co-workers[16] reported superparamagnetic behavior even for on average 10-nm Fe_3O_4 particles encapsulated by a double layer of fatty acids and dispersed in water. In their study the saturating fields for samples with varying volume fractions of particles ranged from 5000 to 10000G. Interestingly, in a study of amorphous Fe_2O_3 particles produced by sonochemical synthesis, Shafi et al.[17] reported a lack of saturation magnetization even up to a field of 18000 G. They also

(14) *CRC Handbook of Chemistry and Physics*; CRC Press: Boca Raton, FL.
(15) Bean, C. P.; Livingston, J. D. *J. Appl. Phys.* **1959**, *30*, 120S.
(16) Shen, L.; Laibinis, P. E.; Hattan, A. T. *Langmuir* **1999**, *15*, 447.
(17) Shafi, K. V. P. M.; Ulman, A.; Yan, X.; Yang, N.-L.; Estournes, C.; White, H.; Rafailovich, M. *Langmuir* **2001**, *17*, 5093.

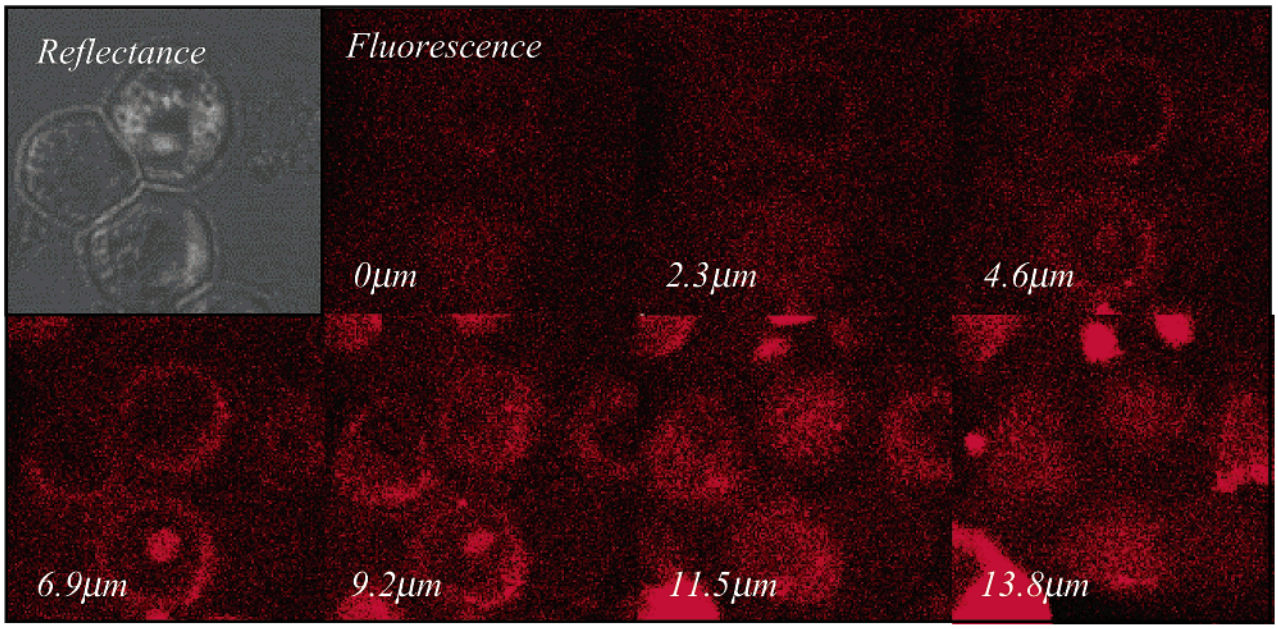

Figure 6. Laser scanning microscopy showing uptake of nanoclinics by KB cells. Optical sections (2.3 μm) of the cells were obtained after 15 min of incubation with LH−RH-positive nanoclinics.

show that phosphonate-coated particles are strikingly different from the ones coated with sulfonate and undecenoate, though it is not clear from their study what role exactly the surfactants might play. In our study, we see magnetization saturation probably because the particles have an ample rotational degree of freedom within the magnetic fluid. Studies detailing the magnetic response of the free particles vs the cell-bound particles are currently underway. Depending on the strength of bonding, we predict a change in the blocking temperature and a distinct difference between the two in the relaxation dynamics in an ac field.

Characterization of Interaction of Nanoclinics with Cells. These multifunctional magnetic nanoclinics were fabricated to target specific cancer cells. The optical probe of the nanoclinic absorbs two photons at 800 nm and emits one photon at ≈580 nm. Because of the encapsulation of the ASPI provided by the silica shell, which minimizes the nonradiative decay pathways induced by the surrounding water molecules, luminescence intensity of the two-photon dye is increased 20 times. This leads to a higher fluorescence quantum efficiency after two-photon absorption.[11] A three-dimensional image of the cells was created by recording different sections with varying depths. Internalization of nanoclinics is observed in LH−RH receptor positive KB cells (Figure 6). This figure shows the particles partitioning in the cell volume after 15 min of incubation at 37 °C. After 30 min of incubation, the cells are saturated with particles and all of the cellular volume shows fluorescence. Experiments performed using CV1 cells (control cells lacking the receptor for LH−RH) did not show any such binding or accumulation. Similarly, KB cells incubated with nanoclinics devoid of LH−RH (control nanoclinics) also failed to show binding or accumulation of particles. These results support the selective targeting action of the nanoclinics and their ability to get a significant number of them inside the cell.

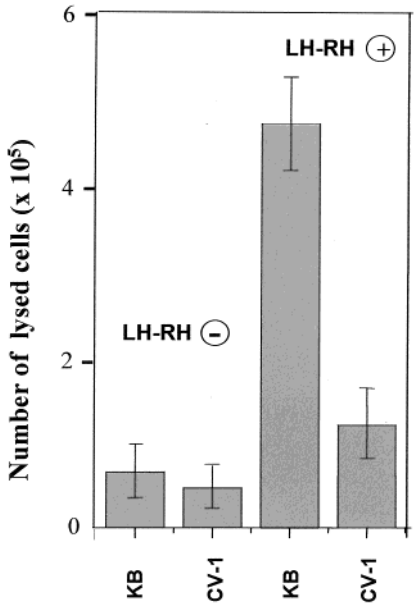

Figure 7. Comparison of magnetocytolytic activity of LH−RH-positive and LH−RH-negative nanoclinics on KB and receptor negative CV-1 cells. Bars represent the standard deviation obtained from three separate experiments.

The ability of these nanoclinics to selectively affect magnetocytolysis (lysis of cells in a magnetic field) was investigated in LH−RH receptor positive cells (KB). It was determined that exposure to a dc magnetic field caused no significant change in the cells in the absence of the nanoclinics. In KB, the number of cells lysed by LH−RH-positive nanoclinics was found to be 8 times higher than that occurring in the presence of LH−RH-negative nanoclinics (Figure 7). Incubation of the nanoclinics with cells for 72 h resulted in a 5-fold increase in the number of lysed cells compared to the 2 h of incubation. Similar experiments using CV-1 cells or LH−RH-negative nanoclinics resulted in no effective magnetocytolytic response.

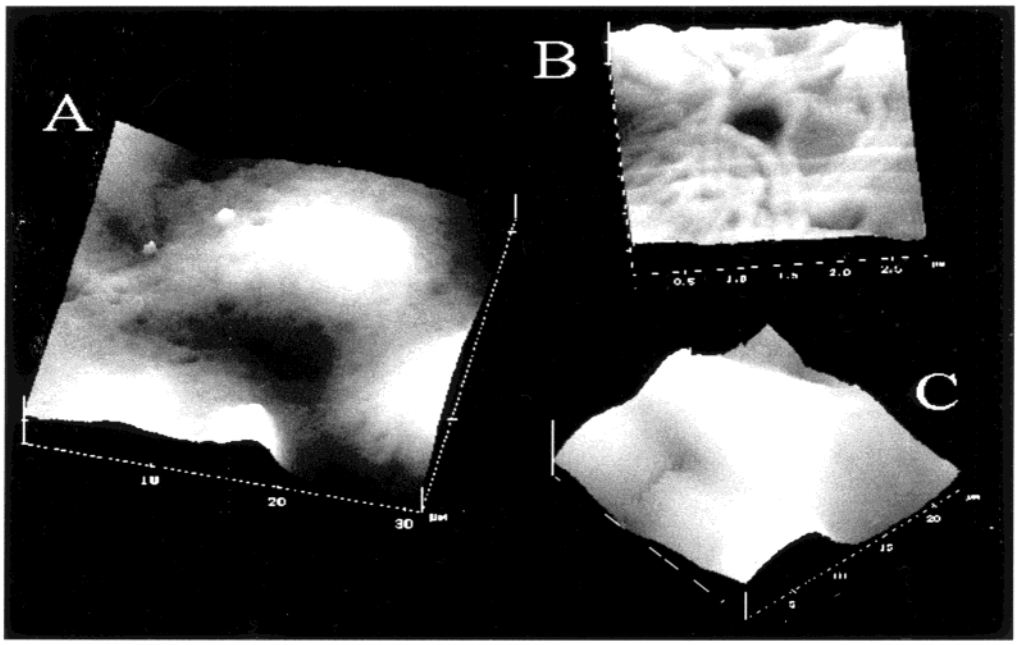

Figure 8. Atomic force microscopy of cells treated with nanoclinics. (A) KB cells incubated with LH−RH-positive nanoclinics. (B) Magnified area of cell surface from A. (C) KB cells treated with LH−RH-negative nanoclinics.

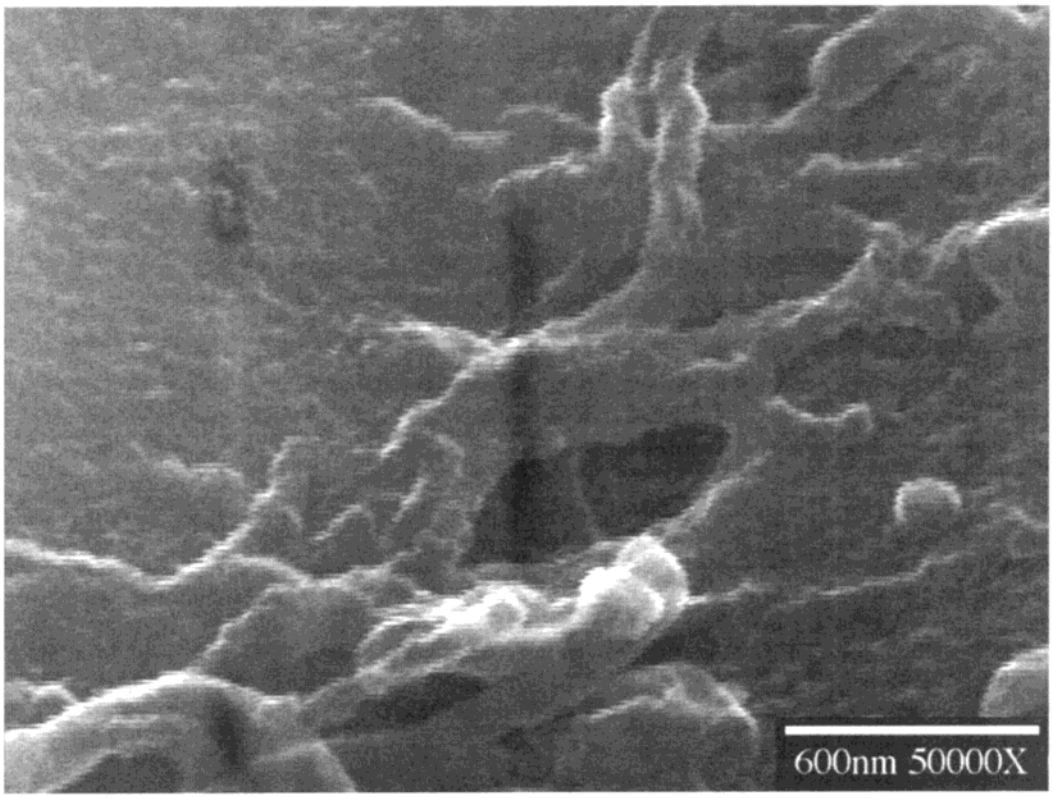

Figure 9. Scanning electron microscopy of KB cells incubated with LH−RH-positive nanoclinics.

Atomic force microscopy (AFM) of KB cells incubated with targeted nanoclinics shows the presence of holes in the membrane of LH−RH receptor-bearing cells after incubation with LH−RH-positive nanoclinics (Figure 8A,B). KB cells incubated with nanoparticles lacking LH−RH did not show any holes in the cell membrane (Figure 8C). The presence of holes in the membrane with LH−RH-positive nanoclinics was confirmed on the KB cell surface using SEM (Figure 9). Elemental analysis (using energy-dispersive spectroscopy) of the areas close to the holes revealed the presence of Fe and Si atoms corresponding to the nanoclinics' composition. These results suggest that the cancer cells are selectively penetrated and destroyed by the magnetic nanoclinics, involving a mechanical disruption of the cell membrane produced by their alignment in a dc magnetic field. Further studies are required to explain the nanoscale interactions between the cell and the particles.

Conclusions

Integration of nanochemistry, targeting systems, and biotechnology have permitted the fabrication of multifunctional nanoparticles or nanoclinics for a new noninvasive diagnostic protocol as well as localized therapy; thus, nanochemistry can play an important role. The selective uptake of the nanoclinics by receptor positive cells, their presence inside these cells, and the physical evidence of "holes" on the cell surface support the proposed ability of these particles to selectively interact and enter specific cancer cells. Combined with the selective lysis of these nanoclinic-loaded cells using a simple dc magnetic field, these nanoclinics can function as diagnostic and therapeutic tools. The nanoclinics can be designed to target selected cancerous tissues, providing a diagnostic analysis and therapy for cancer and infectious diseases from within the cancer cell itself.

Acknowledgment. This work was supported, in part, by the Directorate of Chemistry and Life Sciences of the Air Force Office of Scientific Research, Grant 002239-1-1001693 and, in part, by the National Science Foundation Solid State Chemistry and Polymer program, Grant 010772-1-1001399. We thank Dr. Bruce A. Holm for his valuable discussions and Mr. Peter Bush for his assistance in the SEM and energy-dispersive spectroscopy experiments.

CM0203013